Chinese Chemical Letters 36 (2025) 109597

Contents lists available at ScienceDirect

Chinese Chemical Letters

journal homepage: www.elsevier.com/locate/cclet

One-step synthesis of nanowoven ball-like NiS-WS_2 for high-efficiency hydrogen evolution

Lanfang Wang[1,*], Jiangnan Lv[1], Yujia Li[1], Yanqing Hao, Wenjiao Liu, Hui Zhang, Xiaohong Xu*

Key Laboratory of Magnetic Molecules and Magnetic Information Materials of Ministry of Education, School of Chemical and Material Science, Shanxi Normal University, Taiyuan 030032, China

ARTICLE INFO

Article history:
Received 26 December 2023
Revised 23 January 2024
Accepted 29 January 2024
Available online 3 February 2024

Keywords:
Nanowoven ball-like
Hierarchical
NiS-WS_2
Hydrogen evolution reaction
Synergy

ABSTRACT

Exploring transition metal sulfide electrocatalysts with high-efficiency for hydrogen evolution reaction (HER) is essential to produce H_2 fuel through water splitting. Herein, novel nickel tungsten sulfide heterojunction (NiS-WS_2) with a nanowoven ball-like structure were directed synthetized by a facile hydrothermal method. The hierarchical NiS-WS_2 exhibited excellent HER activity with a relatively small overpotential of 142 and 137 mV at 10 mA/cm^2 in 0.5 mol/L H_2SO_4 and 1 mol/L KOH, which is much better than that of single NiS and WS_2. The impressive performance of NiS-WS_2 heterojunction is owed to the collective synergy of special morphological and more exposed active sites between the crystal interfacial of NiS and WS_2. In addition, the hierarchical NiS-WS_2 can facilitate the transport of charge/mass by optimized electronic structure, which further improves the HER activity of electrocatalysts. These outcomes provide a simple method to prospect towards the design and application of heterostructures as efficient electrocatalysts, shedding some light on the development of functional materials in energy chemistry.

With the continuous progress of science and technology and the rapid growth of global economy, energy crisis has become worldwide issues. Hydrogen energy has received extensive attention because of its high efficiency, cleanliness and renewability [1–4]. For sustainable hydrogen production, electrochemical water splitting is a promising technology, and has been widely studied. As an important reaction for water splitting, hydrogen evolution reaction (HER) usually required additional overpotentials to overcome the slow water decomposition kinetics and unfavorable thermodynamics [5–8]. Therefore, effective HER electrocatalysts with high reaction rates are required to afford high current at low overpotential. Among many hydrogen evolution catalysts, transition metal sulfide (such as WS_2) has received growing attention due to its low price, environmental friendliness and Pt-like electron configuration [9–12]. However, their performance is still inferior to that of Pt-based catalysts for HER [13,14].

To improve the HER catalytic activity of WS_2, several strategies, including morphology engineering and electron structure modulation, have been proposed to overcome the intrinsic activity limitation [15–18]. For example, higher conductivity and more catalytic active sites can be obtained by combining WS_2 with other metal sulfides (such as FeS_2, CoS_2 and Ni_3S_2) to form heterojunction [19–23]. This heterointerface engineering can modulate the electronic properties, as well as chemisorption behavior and composition of catalysts, thereby improving the catalytic efficiency. More importantly, the heterointerface effect can generate new catalytic active centers and charge carriers, which not only increase the number of catalytic active sites, but also promote the mass transport involved in the catalytic reaction. Finally, the kinetic characteristics and adsorption conversion of reactants on the multiphase catalysts were optimized.

Nowadays, prominent progress has been made on the electron structure modulation of Ni-based and W-based sulfide catalysts by heterointerface means [24–28]. And the catalytic performance of multiphase catalysts is superior to their single-component counterpart. However, most of the geometric structures for Ni-based and W-based sulfide catalysts are concentrated in nanosheets, nanorods, nanospheres, as well as their composites [29–31]. Some novel morphologies with more catalytic active sites are neglected. In addition, the Ni-based sulfide with different phase were usually integrated together to enhance their electrochemical properties, and the incorporation of Ni into sulfide catalysts can lead to a distorted structure [1,8,32]. However, the fabrication of these Ni-

* Corresponding authors.
E-mail addresses: lanfang_wang2014@163.com (L. Wang), xuxh@sxnu.edu.cn (X. Xu).
[1] These authors contributed equally to this work.

https://doi.org/10.1016/j.cclet.2024.109597
1001-8417/

based and W-based multiphase sulfides required multisteps, and even desired sulfidation process with poisonous sulfurcontaining gas [33–35]. Therefore, to maximize the catalytic performance of Ni-based and W-based multiphase sulfides, a simple and cost-effective method for the integration of morphology engineering and electronic modulation is highly needed. Especially, the synthesis of nanowoven ball-like polymetallic sulfides for HER remains a significant challenge.

In this paper, a novel nanowoven ball-like NiS-WS_2 with more catalytic active sites were prepared by a simple and cost-effective hydrothermal and annealing treatment. The influence of Ni content on the morphology and catalytic performance of NiS-WS_2 was studied, and the possible catalytic mechanism of the sample was explored. This nanowoven ball-like catalyst has both abundant catalytic active sites and low charge transfer resistance by optimized electronic structure, which further improves the electrocatalytic performance for HER. This work will provide important experimental and theoretical support for revealing the relationship between HER catalytic activity and morphology of the catalyst.

The fabrication process of nanowoven ball-like NiS-WS_2 by one-step hydrothermal method is schematically shown in Fig. 1a. The synthesized samples by the same route with different amount of $NiC_4H_6O_4{\cdot}4H_2O$ (0.15, 0.3, 0.45, 0.6 g) were named as NB1-NiS-WS_2, NB2-NiS-WS_2, NB3-NiS-WS_2 and NB4-NiS-WS_2, respectively. This process does not require complicated equipment and conditions. The crystal structure of WS_2, NiS and NB3-NiS-WS_2 composite was analyzed by X-ray powder diffraction (XRD). As shown in Fig. 1b, the diffraction peaks of WS_2 and NB3-NiS-WS_2 at 28.8°, 33.3°, 39.5°, 43.5°, 48.9°, 58.4°, 60.6° and 69.1° assign to the 2H WS_2 phase (PDF#08–0237). The XRD pattern of NiS and NB3-NiS-WS_2 composite shows diffraction peak at 30.2°, 32.2°, 35.6°, 37.4°, 40.4°, 48.8°, 52.5°, 56.2°, 57.4°, 59.6° and 67.3°, which can be indexed to the β-NiS phase (PDF#12–0041, space group: R3m, $a=b=9.62$ Å and $c=3.15$ Å). Besides, several diffraction peaks of NiS and NB3-NiS-WS_2 composite at 34.4°, 45.9° and 53.4° match well with the crystal planes of α-NiS phase (PDF#02–1280, space group: P63/mmc, $a=b=3.41$ Å and $c=5.32$ Å), confirming the formation of a mixed phase (α-NiS and β-NiS). The XRD patterns of NiS-WS_2 with different Ni precursor were also examined (Fig. S1 in Supporting information). The characteristic peaks of NiS-WS_2 revealed the formation of mixed phase (α-NiS and β-NiS). The excessive Ni precursor gave rise to the increased intensity of NiS phase. For comparison, the Fe-WS_2 and Co-WS_2 were also synthesized by the same route (Supporting information). The incorporation of Fe precursor into WS_2 formed the WS_2-$Fe_{1-x}S$ and WS_2-Fe_3S_4, named as Fe-WS_2 (Fig. S1). And the incorporation of Co precursor formed WS_2-CoS_2 and WS_2-CoS, named as Co-WS_2.

The microstructure of WS_2, NiS-WS_2 and NiS catalyst was observed by scanning electron microscopy (SEM). The SEM image (Fig. 1c) shows that the flower-like WS_2 consist of nanosheets with lengths of microns. While the NiS-WS_2 (Figs. 1d-g and Fig. S2 in Supporting information) with an average size of around 1.2 μm show a semblable spherical appearance, like a nanowoven ball (inset of Fig 1d). Obviously, the spherical structures inherit well while the surface consist of convex prismatic fringes, and many small-sized nanosheets are vertically arranged and closely interconnected with each other to form the convex prismatic fringes. This prismatic fringes on spherical structures provide abundant adhesion points to grow more small-sized nanosheets. These nanosheets exposes more edges active sites on the same volume of nanospheres. As exhibited in Figs. 1d-g, the amount of Ni precursors can effectively control the number and size of small-sized nanosheets. The EDS analysis (Fig. S3 in Supporting information) confirms the presence of Ni, W and S elements in NiS-WS_2, and the ratio of Ni:W has been influenced by the quantity of Ni precursors. By contrast, the surface morphology of NiS in Fig. 1h becomes loose and the irregular structure on the surface stack together. The SEM images of Fe-WS_2 and Co-WS_2 in Fig. S4 (Supporting information) verifies the Ni element are conducive to form nanowoven ball-like structure. Therefore, the nanowoven ball-like NiS-WS_2 heterostructures with highly exposed small-sized nanosheets and abundant edges active sites were successfully synthetized through in situ self-organized strategy.

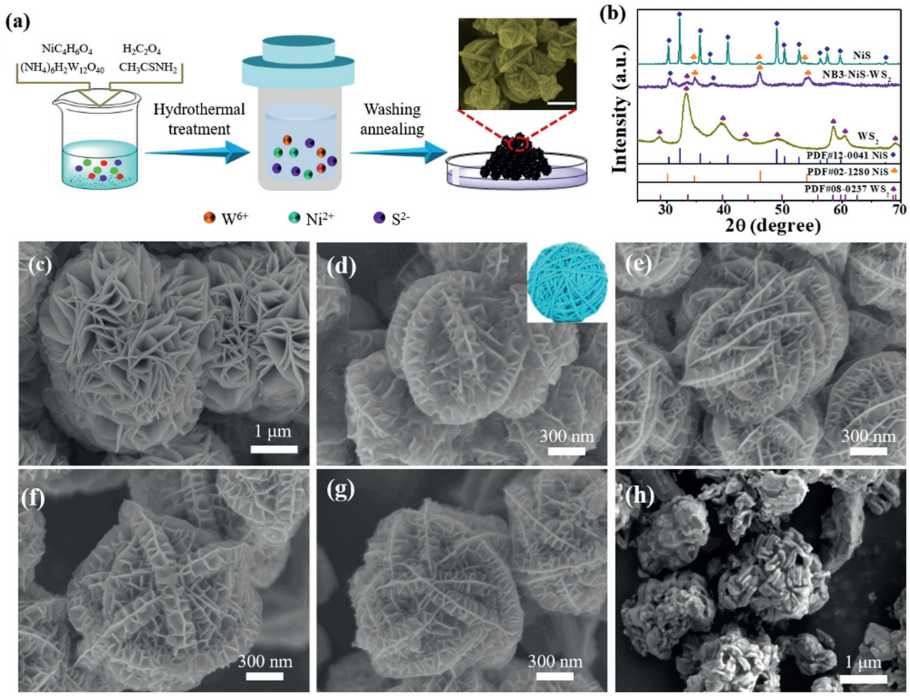

Fig. 1. (a) Illustration for the preparing of nanowoven ball-like NiS-WS_2 by *in situ* self-organized strategy. (b) The XRD images of WS_2, NB3-NiS-WS_2 and NiS. The SEM images of (c) WS_2, (d) NB1-NiS-WS_2, (e) NB2-NiS-WS_2, (f) NB3-NiS-WS_2, (g) NB4-NiS-WS_2 and (h) NiS.

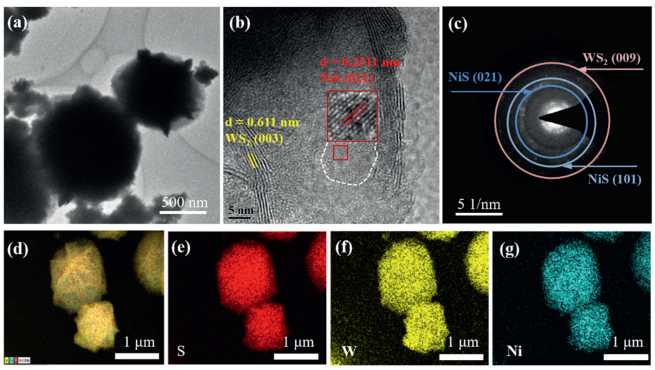

Fig. 2. (a) TEM, (b) HRTEM and (c) SAED images of NB3-NiS-WS_2. (d-g) The mapping diagram of S, W and Ni elements in NB3-NiS-WS_2.

In order to further investigate the microstructures and compositions of nanowoven ball-like NiS-WS_2, transmission electron microscopy (TEM) was performed. Fig. 2a shows that the NB3-NiS-WS_2 have spherical morphology with some nanosheets on the surface. In the high-resolution TEM (HRTEM) image in Fig. 2b, the lattice spacing of 0.611 nm can be clearly observed, which is assigned to (003) plane of WS_2. The lattice fringe with a distance of 0.2511 nm can be assigned to the (021) plane of NiS. The legible interface marked with a white dashed line indicate the existence of a heterointerface between NiS and WS_2. The corresponding selected area electron diffraction (SAED) is displayed in Fig. 2c, the diffraction circles are clearly indexed to NiS and WS_2. Furthermore, the elemental mapping was employed to analyze the atomic arrangement of NB3-NiS-WS_2 catalyst (Figs. 2d-g). The S, W and Ni elements are dispersed homogeneously on the sample. All these results reflect that the incorporation of the Ni and W species modulates the micromorphology of NiS-WS_2 heterostructure to form a uniform nanowoven ball-like NiS-WS_2.

The surface elemental compositions and chemical states of WS_2, NiS and NB3-NiS-WS_2 composite were investigated using X-ray photoelectron spectroscopy (XPS). Fig. 3a exhibits the XPS survey spectra of WS_2, NiS and NB3-NiS-WS_2. The signal of C and O is attributed to CO_2 and oxygen impurities adsorbed on the surface of sample. The high-resolution W 4f spectra of WS_2 and NiS-WS_2 composites (Fig. 3b) displays two sets of spin-split peaks, indicating the presence of W^{4+} and W^{6+} peaks. Here the W^{6+} could be derived from the oxidation of W caused by exposure under the air atmosphere. The different peak positions of W between WS_2 and NB3-NiS-WS_2 suggest that the Ni influences the electronic structure of W, resulting in richer valence states and a negative shift in binding energy. The Ni 2p XPS spectra of NiS and NB3-NiS-WS_2 composite in Fig. 3c is fitted with three sets of peaks, which displays two valence species of Ni^{3+} and Ni^{2+}. Compared to NiS, NB3-NiS-WS_2 exhibits higher energy shifts in the Ni^{2+} and Ni^{3+} peaks, suggesting a decrease in electron density for Ni. Additionally, the S 2p spectrum (Fig. 3d) of NB3-NiS-WS_2 mainly exhibits four different peaks, the peak at 162.1/163.3 eV attributes to S^{2-}, the peak at 169.2/170.4 eV attributes to the peak of S-O. These peaks exhibit a significantly negative shift compared to WS_2 and NiS, implying higher charge density at S sites. These findings suggest a strong interfacial interaction between WS_2 and NiS is generated, leading to the electron transfer from Ni to WS_2. This modifies the electronic properties of the electrocatalyst and optimizes the adsorption and desorption abilities of active species at active sites, consequently improving their HER catalytic activity [36].

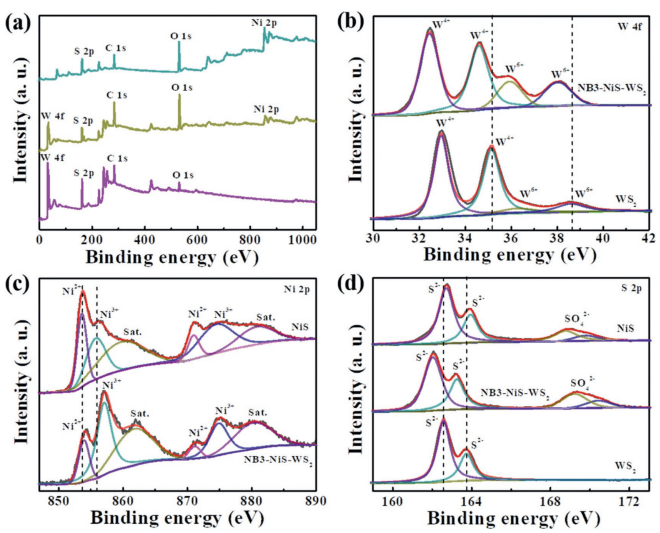

Fig. 3. (a) The XPS survey spectra for WS_2, NiS and NB3-NiS-WS_2. High-resolution XPS spectra of (b) W 4f, (c) Ni 2p and (d) S 2p in WS_2, NB3-NiS-WS_2 and NiS.

The HER activities of the as-prepared catalysts were investigated in 0.5 mol/L H_2SO_4 electrolyte using a standard three-electrode system without iR compensation. Fig. 4a displays linear sweep voltammetry (LSV) curves of different catalysts with a scan rate of 5 mV/s. Clearly, the HER activity of carbon fiber cloth (CF) substrate was low. The various NiS-WS_2 composite catalyst exhibit significant enhancements in the HER (Fig. 4a and Fig. S5 in Supporting information). The polarization curve of the NB3-NiS-WS_2 catalyst exhibits the best HER activity among these catalysts, requiring a low overpotential of 142 mV to achieve the current density of 10 mA/cm^2. This is superior to that of NiS (197 mV) and WS_2 (318 mV). The Tafel slope is used to reflect the kinetic characteristics of the electrocatalyst in HER. As shown in Fig. 4b, Pt/C has the smallest Tafel slope of 47.1 mV/dec, which is attributed to its optimal kinetic advantage. The NB3-NiS-WS_2 composite displays a Tafel slope of 78.6 mV/dec, exhibiting a more rapid HER kinetics than that of NiS (106.3 mV/dec) and WS_2 (141.3 mV/dec) electrocatalysts. The Electrochemical impedance spectroscopy (EIS) measurement was used to evaluate the electrocatalytic kinetics between the interface of electrolyte and electrocatalyst. As exhibited in Fig. S6 (Supporting information), a smaller charge transfer resistance (the diameter of the semicircle) of NB3-NiS-WS_2 imply a faster electron transport kinetic in the hierarchical heterostructure. These results confirm that the Ni doping play an important role in promoting the HER activity of WS_2. Moreover, as exhibited in Fig. 4c, the catalytic performance of NB3-NiS-WS_2 composite surpasses most of the W-based and Ni-based electrocatalysts reported [22,23,37-40].

The electrochemical surface areas (ECSA) of electrocatalysts were evaluated by means of electrochemical double layer capacitance (C_{dl}) tests. The cyclical voltammetry (CV) measurement with different scan rate was used to calculate the C_{dl} (Fig. 4d and Fig. S7 in Supporting information). As displayed in Fig. 4e, the NB3-NiS-WS_2 electrocatalyst exhibits a C_{dl} value of 45.3 mF/cm^2, higher than those of WS_2 (8.5 mF/cm^2), NiS (1.9 mF/cm^2), and CF (0.22 mF/cm^2). This suggests the electrochemical active area of the prepared NB3-NiS-WS_2 catalyst is the largest, which is consistent with the N_2 adsorption–desorption result in Fig. S8 (Supporting information) and the HER catalytic activity in Fig. 4a. Fig. 4f shows the LSV curves of NB3-WS_2_NiS before and after 300 cycles. It can be observed that the sample almost has no HER current loss, suggesting a good stability. These results suggest that the smaller charge transfer resistance and larger ECSA of the special nanowoven ball-like structure account for the excellent HER performance of NB3-NiS-WS_2.

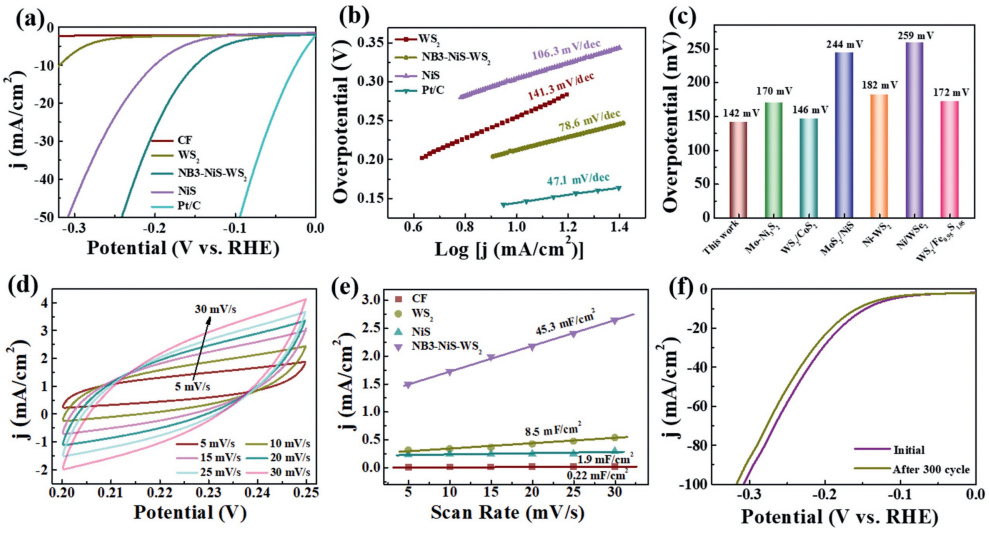

Fig. 4. (a) LSV curves of NB3-NiS-WS_2, WS_2, NiS, commercial Pt/C and blank CF. (b) Tafel plots for different catalysts *vs.* RHE. (c) The comparison of HER performance with recently reported Ni-based and W-based catalysts. (d) CV curves of NB3-NiS-WS_2 with different scan rate. (e) C_{dl} for different catalysts. (f) LSV curves of BN3-NiS-WS_2 before and after 300 cycles.

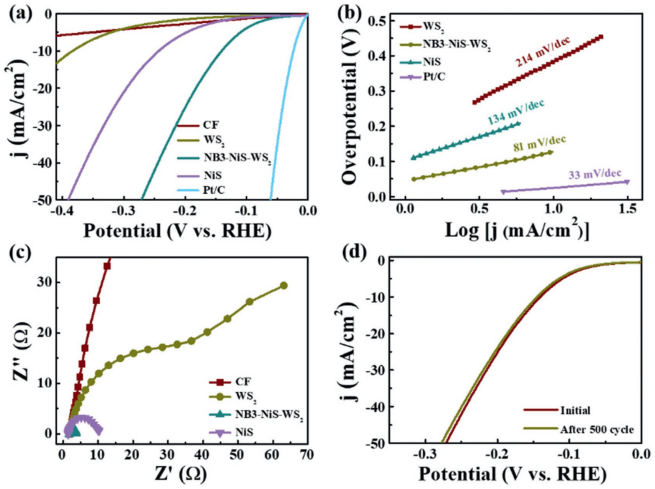

Fig. 5. (a) LSV curves at 2 mV/s in 1 mol/L KOH. (b) Tafel slope and (c) EIS curves for different catalysts. (d) LSV curves of NB3-NiS-WS_2 before and after 500 cycles.

We further evaluated the HER performance of BN3-NiS-WS_2 and the control catalysts in alkaline media (1 mol/L KOH). Fig. 5a shows that BN3-NiS-WS_2 exhibits excellent electrocatalytic behavior for HER ($\eta_{10} = 137$ mV), exceeding NiS ($\eta_{10} = 241$ mV), WS_2 ($\eta_{10} = 381$ mV) and other WS_2-based catalysts (Fig. 5a and Fig. S9 in Supporting information). The dynamic process related with the Tafel slope can also be used to reveal the improved HER performance. As shown in Fig. 5b, the NB3-NiS-WS_2 catalyst displays a Tafel slope of 81 mV/dec, much smaller than that of NiS (134 mV/dec), WS_2 (214 mV/dec), indicating the largest catalytic reaction kinetics. The interfacial charge-transfer kinetics was elucidated by means of EIS measurements. As exhibited in Fig. 5c, the four curves have similar changing trends and are all composed of semi-circles in the high frequency region. The low charge transfer resistance of NB3-NiS-WS_2 suggests the rapid catalytic reaction kinetics for HER at the electrocatalyst/electrolyte interface. Therefore, the excellent HER performance of NB3-NiS-WS_2 is mainly due to the abundant edge active sites and interfaces on the special nanowoven ball-like structure, which improving the intrinsic electronic conductivity. The stability of the NB3-NiS-WS_2 is finally elucidated by using the LSV curves (Fig. 5d) before and after 500 cycle CV measurement. The LSV curve remains almost the same as the initial curve. These results indicate that the NB3-NiS-WS_2 electrocatalyst exhibits an outstanding and robustness HER performance in the alkaline solution.

In conclusion, a novel nanowoven ball-like NiS-WS_2 were successfully prepared through a simple and scalable hydrothermal process. The surface of the as-prepared NB3-NiS-WS_2 catalyst consists of convex prismatic fringes, and many small-sized nanosheets are vertically arranged and closely interconnected with each other to form the convex prismatic fringes. This NB3-NiS-WS_2 catalyst exhibited an excellent HER activity and stability in both acid and alkaline solutions. The excellent HER activity is mainly due to the abundant edge active sites and interfaces on the same volume of nanospheres, which improving the intrinsic electronic conductivity. This facile and scalable method can open the door for the discovery of low-cost electrocatalyst.

Declaration of competing interest

The authors declare that they have no known competing financial interests or personal relationships that could have appeared to influence the work reported in this paper.

Acknowledgments

The work is financially supported by the National Natural Science Foundation of China (No. 52202340), the Scientific and Technological Innovation Programs of Higher Education Institutions in Shanxi (No. 2021L266), the Applied Basic Research Project of Shanxi Province (No. 20210302124425) and the Graduate Science and Technology Innovation Project Foundation of Shanxi Normal University (No. 2023XSY065).

Supplementary materials

Supplementary material associated with this article can be found, in the online version, at doi:10.1016/j.cclet.2024.109597.

References

[1] T. Sun, Z. Tang, W. Zang, et al., Nat. Nanotechnol. 18 (2023) 763–771.

[2] J. Baek, M.D. Hossain, P. Mukherjee, et al., Nat. Commun. 14 (2023) 5936.
[3] G. Li, H. Jang, S. Liu, et al., Nat. Commun. 13 (2022) 1270.
[4] Z. Lei, W. Cai, Y. Rao, et al., Nat. Commun. 13 (2022) 24.
[5] J. Ge, D. Zhang, Y. Qin, et al., Appl. Catal. B: Environ. 298 (2021) 120557.
[6] J. Li, Y. Zhang, C. Liu, et al., Adv. Funct. Mater. 32 (2021) 2108316.
[7] B. Fei, Z. Chen, J. Liu, et al., Adv. Energy Mater. 10 (2020) 2001963.
[8] W. Xu, R. Zhao, Q. Li, et al., Adv. Energy Mater. 13 (2023) 2300978.
[9] Y. Yang, H. Yao, Z. Yu, et al., J. Am. Chem. Soc. 141 (2019) 10417–10430.
[10] X. Ma, J. Li, C. An, et al., Nano Res. 9 (2016) 2284–2293.
[11] A. Han, X. Zhou, X. Wang, et al., Nat. Commun. 12 (2021) 709.
[12] Y. Jing, X. Mu, C. Xie, et al., Int. J. Hydrog. Energy 44 (2019) 809–818.
[13] L. Sun, M. Gao, Z. Jing, et al., Chem. Eng. J. 429 (2022) 132187.
[14] M. Ma, J. Xu, H. Wang, et al., Appl. Catal. B: Environ. 297 (2021) 120455.
[15] L. Liu, C. Zhang, M. Chen, et al., Appl. Surf. Sci. 573 (2022) 151606.
[16] S. Peng, L. Li, J. Zhang, et al., J. Mater. Chem. A 5 (2017) 23361–23368.
[17] L. Wang, R. Yang, J. Fu, et al., Rare Metals 42 (2023) 1535–1544.
[18] J. Tan, S. Li, B. Liu, et al., Small Struct. 2 (2020) 2000093.
[19] H.L. Chen, Y.Q. Li, H.Y. Huang, et al., Energy Fuel 36 (2022) 4888–4894.
[20] D.R. Paudel, U.N. Pan, R.B. Ghising, et al., Nano Energy 102 (2022) 107712.
[21] Z.Q. Zhang, X.F. Lin, S.L. Tang, et al., Int. J. Hydrog. Energy 47 (2022) 33643–33651.
[22] J. Wu, T. Chen, C. Zhu, et al., ACS Sustain. Chem. Eng. 8 (2020) 4474–4480.
[23] L. Sun, J. Geng, M. Gao, et al., Chem. Eur. J. 27 (2021) 10998–11004.
[24] W.J. Jiang, T. Tang, Y. Zhang, et al., Acc. Chem. Res. 53 (2020) 1111–1123.
[25] E. Meza, R.E. Diaz, C.W. Li, ACS Nano 14 (2020) 2238–2247.
[26] P.V. Sarma, A. Kayal, C.H. Sharma, et al., ACS Nano 13 (2019) 10448–10455.
[27] W. Xu, C. Zhang, H. Shen, et al., ACS Sustain. Chem. Eng. 10 (2022) 14396–14406.
[28] W. Han, Z. Liu, Y. Pan, et al., Adv. Mater. 32 (2020) 2002584.
[29] Q. Fu, J. Han, X. Wang, et al., Adv. Mater. 33 (2021) 1907818.
[30] R. He, C. Wang, L. Feng, Chin. Chem. Lett. 34 (2023) 107241.
[31] K. Zhang, Y. Duan, N. Graham, et al., Appl. Catal. B: Environ. 323 (2023) 122144.
[32] H. Wei, J. Si, L. Zeng, et al., Chin. Chem. Lett. 34 (2023) 107144.
[33] H. Wang, J. Xu, Q. Zhang, et al., Adv. Funct. Mater. 32 (2022) 2112362.
[34] W. Hong, E. Meza, C.W. Li, J. Mater. Chem. A 9 (2021) 19865–19873.
[35] B. Qiu, Y. Zhang, X. Guo, et al., J. Mater. Chem. A 10 (2022) 719–725.
[36] W. Antink, S. Lee, H. Lee, et al., Adv. Funct. Mater. 34 (2023) 2309438.
[37] J. Li, Z. Yang, Y. Lin, et al., New J. Chem. 44 (2020) 8578–8586.
[38] Q. Qin, L. Chen, T. Wei, et al., Small 15 (2019) 1803639.
[39] X. Zhang, P. Yang, S.P. Jiang, Carbon 175 (2021) 176–186.
[40] S.R. Kadam, A.N. Enyashin, L. Houben, et al., J. Mater. Chem. A 8 (2020) 1403–1416.